Research Square

Preprints are preliminary reports that have not undergone peer review.
They should not be considered conclusive, used to inform clinical practice,
or referenced by the media as validated information.

Meteorological factors and haemorrhagic fever with renal syndrome incidence in ten provinces of China, 2005–2020: a two-stage, age- stratified distributed lag non-linear analysis

Fei Wang
First Affiliated Hospital of Xi'an Jiaotong University
Minghui Tai
First Affiliated Hospital of Xi'an Jiaotong University
Mi Ke
First Affiliated Hospital of Xi'an Jiaotong University
Yuxin Liu
First Affiliated Hospital of Xi'an Jiaotong University
Yuanyuan Duan
Xian Center for Disease Control and Prevention
Tianyan Chen
First Affiliated Hospital of Xi'an Jiaotong University
Zhen Tian
tianzhen@xjtufh.edu.cn

First Affiliated Hospital of Xi'an Jiaotong University

Research Article

Keywords: Hemorrhagic fever with renal syndrome, Hantavirus, Temperature, Precipitation, Relative humidity, Distributed lag non-linear model, Multivariate meta-analysis, Age stratification, China

Posted Date: October 27th, 2026

DOI: https://doi.org/10.21203/rs.3.rs-11302260/v1

License: This work is licensed under a Creative Commons Attribution 4.0 International License. Read Full License

Additional Declarations: No competing interests reported.

Abstract

Background

Haemorrhagic fever with renal syndrome (HFRS) is a rodent-borne zoonosis with its largest burden in China. Meteorological conditions influence transmission, but age- and endemic-type-specific associations remain unclear, and most multi-region studies lack population denominators.

Methods

We analysed 132,313 age-stratified HFRS cases reported during 2005–2020 in ten Chinese provinces, grouped by reservoir-host seasonality into Apodemus-type, Mixed-type and Rattus-type regions. Population denominators came from three censuses and revised intercensal series; monthly meteorological exposures came from quality-controlled national stations. Within each province and age stratum (0–19, 20–59, ≥ 60 years), we fitted quasi-Poisson distributed lag non-linear models (lag 0–6 months) with a log person-month offset and mutual exposure adjustment, pooling reduced curves by endemic type and stratum. Curve robustness was assessed using best linear unbiased predictions and a 2,000-draw bootstrap; null results were bounded by minimum detectable relative risks; provincial covariates were examined in meta-regressions.

Results

The 20–59-year stratum contributed 75.8% of cases (annual incidence 1.70 per 100,000, versus 0.33 at 0–19 and 1.57 at ≥ 60 years). In Apodemus-type provinces, precipitation showed an inverted-U association peaking at 175.9 mm (relative risk (RR) 2.73, 95% CI 1.44–5.18), strongest at ages 20–59 (190.6 mm, RR 3.08, 1.14–8.37) and robust to leave-one-province-out analysis (95th-percentile RR 1.44–3.52). Temperature peaked near 8.7°C (RR 1.44, 0.34–6.01). Humidity associations were weak on average but diverged across climate zones (dry-promoting in Shaanxi versus humid-promoting in Shandong), producing near-flat pooled curves (I^2 up to 72.8%). The two Rattus-type provinces showed opposite temperature-curve directions (heat-promoting in subtropical Yunnan, cold-promoting in temperate Hebei) and are therefore reported per province. Age stratification eliminated Apodemus-type precipitation heterogeneity in the 0–19 and ≥ 60 strata (I^2 = 0%). Provincial ageing rate explained temperature-curve heterogeneity (P = 0.004; I^2 reduced from 60.0% to 40.2%). Detectability bounds indicated adequate power for moderate precipitation effects at working ages, but not for temperature extremes in sparse strata.

Conclusions

Meteorological–HFRS associations are structured by reservoir-host endemic type, concentrated in the working-age population, and modified by population ageing. Age-stratified designs with population denominators are essential for unbiased multi-region synthesis.

Background

Haemorrhagic fever with renal syndrome (HFRS) is a rodent-borne zoonosis caused by Old World hantaviruses, principally Hantaan virus (HTNV), carried by the striped field mouse (Apodemus agrarius), and Seoul virus (SEOV), carried by the brown rat (Rattus norvegicus) [1]. China bears the largest share of the global burden, with HFRS classified as a class B notifiable disease and transmission sustained across most provinces [2, 3]. The two dominant reservoir hosts have distinct ecology and seasonality: A. agrarius is a field-dwelling species driving autumn–winter peaks in rural areas, whereas R. norvegicus is commensal and typically drives spring peaks; many provinces host mixed transmission [2].

Climatic conditions act on all components of the transmission cycle — reservoir density and behaviour, virus survival in the environment, and human–rodent contact — and a substantial literature has linked HFRS incidence to temperature, precipitation and humidity at city and provincial scales [4–12]. Most recently, a nationwide case-crossover analysis of 285 cities (202,154 cases, 2005–2022) showed that temperature and humidity associations differ systematically across epidemic regions defined by reservoir-host seasonality, with subgroup analyses suggesting effect modification by age [13], indicating that single national summaries obscure regionally and demographically distinct, potentially opposite, exposure–response relationships.

Four gaps remain. First, age structure: HFRS incidence and severity are strongly age-dependent, and the subgroup analyses of the nationwide study suggested that age modifies the temperature association [13]; however, those analyses compared case-count odds ratios across age groups without age-specific population denominators, so age-specific incidence-rate curves remain unestimated. Second, denominators: many distributed lag non-linear model (DLNM) studies of HFRS model raw case counts without population offsets, conflating demographic change with incidence risk; this matters particularly in China, where provincial populations were revised substantially after the 2020 census. Third, scale and typing: percentile-scale pooling, although convenient across climate zones, discards the absolute exposure levels needed for public-health thresholds, and pooling has rarely been organised by reservoir-host endemic type, the biological axis along which transmission seasonality is defined. Fourth, timescale and exposure scope: the nationwide analysis resolved daily exposures over lags of up to 60 days — a window centred on the incubation period — and did not include precipitation in its main models; monthly-scale analyses with lags of up to six months are needed to capture reservoir-population-mediated effects and to estimate absolute precipitation thresholds.

We therefore conducted a two-stage, age-stratified DLNM analysis of 132,313 HFRS cases reported during 2005–2020 in ten Chinese provinces spanning 25.0°N to 45.8°N, with census-anchored population denominators, quality-controlled station-based meteorological exposures on absolute scales, and pooling by endemic type and age stratum. We quantified the robustness of province-level curve shapes using best linear unbiased predictions (BLUPs) and a parametric bootstrap, bounded null results with minimum detectable effects, and examined province-level demographic and climatic drivers of heterogeneity in meta-regressions.

Methods

Study design and setting

We conducted an ecological monthly time-series analysis in ten provinces of mainland China — Heilongjiang, Shaanxi, Shandong, Jiangxi, Henan, Liaoning, Hunan, Sichuan, Yunnan and Hebei — selected as the leading HFRS-endemic provinces for which quality-controlled daily meteorological series were available. The study period was January 2005 to December 2020 (192 months). The units of analysis were province × calendar month × age stratum. The provinces span 21 degrees of latitude, from the mid-temperate northeast (Heilongjiang; centroid 45.8°N, mean annual temperature 2.7°C) to the subtropical southwest (Yunnan; 25.0°N, 16.6°C) (Table 1). Following the reservoir-host seasonality of the dominant hantaviruses [2] and the seasonal classification approach of Chang et al. [13], which distinguishes spring-peak (March–July) from autumn–winter-peak (September–January) transmission, provinces were grouped into three endemic types: Apodemus-type (autumn–winter peak; Heilongjiang, Shaanxi, Shandong, Jiangxi, Henan), Mixed-type (Liaoning, Hunan, Sichuan) and Rattus-type (spring peak; Yunnan and Hebei).

Table 1
Study provinces: endemic type, HFRS cases 2005–2020, and provincial covariates

Province	Endemic type	Cases	Latitude (°N)	MAT (°C)	Spring-peak share (%)	Urbanisation 2020 (%)	≥ 60 y share 2020 (%)	Ageing rate (pp/y)
Heilongjiang	Apodemus-type	30276	45.8	2.67	37.3	65.61	23.22	0.817
Liaoning	Mixed-type	19442	41.8	8.97	49.4	72.14	25.72	0.812
Hebei	Rattus-type	10134	38.64	12.31	57.6	60.07	19.85	0.543
Shandong	Apodemus-type	19727	36.65	13.3	33.1	63.05	20.9	0.51
Shaanxi	Apodemus-type	26677	34.34	12.08	20.3	62.66	19.2	0.528
Hunan	Mixed-type	9935	28.23	17.6	42.9	58.76	19.88	0.463
Jiangxi	Apodemus-type	8443	28.68	18.33	36.8	60.44	16.87	0.431
Henan	Apodemus-type	3785	34.75	15.43	30.0	55.43	18.08	0.437
Sichuan	Mixed-type	1894	30.57	12.05	44.4	56.73	21.71	0.523
Yunnan	Rattus-type	2000	25.04	16.63	53.2	50.05	14.91	0.319

MAT: mean annual temperature 2005–2020; spring-peak share: proportion of annual cases occurring in March–July; ageing rate: annualised percentage-point change in the ≥ 60-year population share, 2005–2020. Apodemus-type: autumn–winter-peak, field-rodent-dominated; Mixed-type; Rattus-type: spring-peak, commensal-rodent-dominated (Yunnan and Hebei). Provinces ordered by latitude.

Case data and age stratification

Monthly counts of HFRS cases by age group were obtained from the Data-center of China Public Health Science (National Population Health Data Center), which compiles cases reported through the national notifiable infectious disease surveillance system [14]. Cases were aggregated into three age strata — 0–19, 20–59 and ≥ 60 years — chosen to separate children and adolescents, the occupationally exposed working-age population, and older adults. Records with unknown age (one record in Hebei) were excluded from the analytic dataset. Provincial case summaries are provided in Additional file 1 (Note S1 and Table S1).

Population denominators

Age-specific population denominators were constructed from the five-year age pyramids of the 2000, 2010 and 2020 national population censuses [15], with the officially revised year-end resident population series as total controls. Provincial totals were interpolated geometrically between census anchors; age-group shares were taken from census tabulations and interpolated linearly between censuses; monthly person-time was obtained by linear interpolation of annual populations. Validation against published figures showed reconstruction errors of at most 0.11% in census years and deviations of 0.2–1.8 percentage points from statistical-bulletin age shares; differences from unrevised bulletins in 2019 (for example − 13.6% in Heilongjiang) reflect the post-2020-census revisions and are by design. Incidence rates are expressed per 100,000 person-years. Full construction and validation details are given in Additional file 1 (Note S2).

Meteorological data and quality control

Daily surface observations were obtained from the China Meteorological Data Sharing Service System (dataset SURF_CLI_CHN_MUL_DAY, version 3.0) for 388 national meteorological stations within the ten provinces (17–38 stations per province, except Hebei, for which a fuller station extract yielded 141 stations meeting the same inclusion rules) [16]. We extracted daily mean air temperature (°C), daily precipitation (0.1 mm) and daily mean relative humidity (%). Instrument quality-control flags were applied: records flagged as erroneous were discarded (four daily records in total); trace precipitation and the no-precipitation codes were set to zero; missing codes were set to missing. Monthly means (temperature, humidity) and monthly totals (precipitation) were computed when at least 25 valid daily records were available (excluding approximately ten station-months), and provincial exposures were the unweighted means across stations; one province-month (Jiangxi, May 2014) was interpolated from neighbouring months, and no interpolation was required for Hebei. Exposure series constructed under this quality-control protocol were virtually identical to those of a preliminary build (Pearson r = 1.000). Processing details and station counts are given in Additional file 1 (Note S3 and Table S2).

Stage 1: province- and stratum-specific DLNMs

For each province × age stratum × exposure combination (10 × 4 strata including all ages × 3 exposures), we fitted a quasi-Poisson generalized linear model with a distributed lag non-linear cross-basis [17, 18],

including the logarithm of stratum-specific person-months as an offset so that incidence rates were modelled directly. The exposure dimension used a natural cubic spline with internal knots at the 25th and 75th percentiles of the pooled ten-province exposure distribution (6.12 and 21.24°C for temperature; 15.72 and 117.91 mm for precipitation; 60.3% and 76.3% for humidity) and boundary knots at the pooled minimum and maximum; curves were centred at the pooled median (14.38°C, 52.8 mm and 68.6%, respectively). The lag dimension covered 0–6 months with a natural cubic spline (3 df). Each exposure model was mutually adjusted for the other two exposures as natural splines (3 df each), for seasonality through calendar-month indicators, and for long-term trends through a natural cubic spline of time (32 df over 192 months, approximately 2 df per year). Convergence settings were tightened (maximum 200 iterations; tolerance 1 × 10 − 7). Cumulative exposure–response associations over the entire lag window were derived by cross-basis reduction; estimated dispersion parameters ranged from 0.4 to 5.6 and were accommodated by the quasi-Poisson family. The full specification is summarised in Additional file 1 (Note S4).

Stage 2: multivariate meta-analysis by endemic type

The reduced coefficient vectors (with variance–covariance matrices) were pooled with random-effects multivariate meta-analysis using restricted maximum likelihood [19, 27], separately within each endemic type × age stratum combination and across all ten provinces; maximum likelihood was used for one Rattus-type fit in which restricted maximum likelihood did not converge. The two Rattus-type provinces (Yunnan and Hebei) showed opposite stage-1 temperature-curve directions and their pooled estimates were unstable (I^2 up to 83.9%); Rattus-type results are therefore reported per province from stage-1 estimates, without random-effects pooling. Between-province heterogeneity was assessed with the multivariate Cochran's Q test and the I^2 statistic. Province-specific BLUPs were computed to summarise shrunken estimates, and leave-one-province-out (LOPO) analyses repeated the pooling excluding one province at a time.

Curve-shape classification and parametric bootstrap

Because BLUP shrinkage towards the pooled mean can in principle reverse the direction of a province-level curve, we assessed shape robustness directly. Each province- and stratum-specific curve was classified from the mean log relative risk over the cold tail (within-province exposure percentiles P1–P25) and the hot tail (P75–P99): cold-promoting when the cold-tail mean exceeded zero and the hot-tail mean did not; heat-promoting vice versa; U-shaped when both tail means exceeded zero; and mid-peak (inverted-U) when both were below zero (for humidity, the tails correspond to dry and humid conditions). Sampling variability of the shape was quantified by a parametric bootstrap: 2,000 draws from the stage-1 reduced coefficient distribution $N(\beta, \hat{V})$ per province and stratum, each reconstructed to a full curve and re-classified. We report the probability of retaining the raw stage-1 shape, the probabilities of each tail direction, and the probabilities that the relative risks at P5 and P95 exceed 1. Further details are given in Additional file 1 (Note S5).

Detectable effects for null results

To bound null findings, we computed the minimum detectable relative risk (MDR) — the smallest RR detectable with 80% power at two-sided α = 0.05 given the pooled standard error, exp[(z0.975 + z0.80) × SE] — at the 5th and 95th exposure percentiles, and the minimum detectable effect (MDE) for between-stratum RR ratios, combining stratum-specific standard errors under independence. Details are given in Additional file 1 (Note S6).

Drivers of heterogeneity

Eight province-level covariates were examined in univariate multivariate meta-regressions: centroid latitude; mean annual temperature (2005–2020); spring-peak share (proportion of annual cases occurring in March–July); urbanisation rate in 2020; the ≥ 60-year population share in 2005 and 2020; the annualised ageing rate (percentage-point change per year in the ≥ 60 share between 2005 and 2020); and endemic type. For each covariate, a joint Wald test assessed whether the whole curve varied with the covariate. These analyses rest on at most ten provinces and are exploratory.

Software and ethics

Analyses used R version 4.6.1 with packages dlnm, mixmeta and splines. The study used aggregated, anonymised surveillance counts and publicly available census and meteorological data; no individually identifiable information was accessed, and ethical approval and informed consent were not required.

Results

Descriptive statistics

A total of 132,313 HFRS cases were reported in the ten provinces during 2005–2020 (Table 1). The 20–59-year stratum accounted for 75.8% of cases (100,292), against 6.2% (8,204) at ages 0–19 and 18.0% (23,817) at ages ≥ 60; crude annual incidence was 1.70, 0.33 and 1.57 per 100,000 person-years, respectively, so the working-age burden was 5.1-fold that of children and adolescents. Case numbers were largest in Heilongjiang (30,276), Shaanxi (26,677), Shandong (19,727) and Liaoning (19,442), with Hebei contributing a further 10,134. The climatic gradient across provinces was pronounced (mean annual temperature 2.7°C in Heilongjiang to 18.3°C in Jiangxi), as was the demographic gradient (≥ 60-year population share in 2020 from 14.9% in Yunnan to 25.7% in Liaoning; annualised ageing rate 0.32–0.82 percentage points per year).

Temperature

In Apodemus-type provinces, the pooled cumulative temperature–incidence curve was an inverted U peaking at 8.7°C (RR 1.44, 95% CI 0.34–6.01), declining towards both tails (RR at the 95th percentile, 27.1°C, 0.37, 95% CI 0.03–4.21) (Fig. 1a; Table 2). The all-ten-province pooled curve was similar (peak 7.4°C, RR 1.61, 95% CI 0.40–6.53) (Table 2). Point estimates departed from 1 but confidence intervals were wide, reflecting substantial between-province heterogeneity (all-ages I^2 = 50.0% in Apodemus-type provinces). The Mixed-type pooled curve was unstable with very wide intervals (Fig. 1c). The two Rattus-type provinces showed opposite temperature shapes and are reported per province (Additional file 1: Fig. S1). In Yunnan, the stage-1 curve was heat-promoting and among the most robust single-province shapes: at ages 20–59

the bootstrap probability of retaining the heat-promoting shape was 0.902, the heat-direction probability 0.913, and the probability that RR exceeded 1 at the 95th percentile 0.917, with the shape unchanged under BLUP shrinkage (Table 4; Additional file 1: Table S6). In Hebei, by contrast, temperature curves were cold-promoting in all three age strata — most decisively at ages ≥ 60, where the cold-direction probability was 0.963 and the probability that RR exceeded 1 at the 5th percentile was 0.980 (Table 4; Additional file 1: Table S6).

Table 2
Pooled cumulative relative risks at curve peaks and 95th percentiles, lag 0–6 months

Exposure	**Group / stratum**	**Peak RR (95% CI; peak location)**	**RR at P95 (95% CI)**
Temperature	Apodemus-type, all ages	1.44 (95% CI 0.34–6.01); 8.7°C	0.37 (95% CI 0.03–4.21)
Temperature	All ten provinces, all ages	1.61 (95% CI 0.40–6.53); 7.4°C	0.30 (95% CI 0.07–1.35)
Precipitation	Apodemus-type, all ages	2.73 (95% CI 1.44–5.18); 175.9 mm	2.23 (95% CI 0.66–7.51)
Precipitation	Apodemus-type, 20–59 y	3.08 (95% CI 1.14–8.37); 190.6 mm	2.84 (95% CI 0.58–13.87)
Precipitation	All ten provinces, all ages	1.78 (95% CI 0.99–3.20); 168.6 mm	1.53 (95% CI 0.69–3.39)
Relative humidity	All ten provinces, all ages	—	1.24 (95% CI 0.71–2.15)

Cumulative RRs over lags of 0–6 months from two-stage random-effects multivariate meta-analysis on absolute exposure scales, centred at the pooled median (14.38°C; 52.8 mm; 68.6%). P95: 95th percentile of the pooled exposure distribution (Apodemus-type: 27.1°C and 224.5 mm; all ten provinces: 26.7°C, 223.4 mm and 82.6%). The two Rattus-type provinces (Yunnan and Hebei) showed opposite curve directions and are reported per province (see text and Additional file 1: Fig. S1).

Table 4
Parametric bootstrap shape-robustness results for selected province–stratum cells

Province / exposure	Stratum	Raw shape	BLUP shape	P(retained)	P(direction)	P(RR > 1)
Yunnan / temperature	20–59 y	Heat-promoting	Heat-promoting	0.902	0.913 (heat)	0.917 at P95
Henan / precipitation	0–19 y	Cold-promoting	Cold-promoting	0.821	0.919 (dry)	0.967 at P5
Shaanxi / humidity	20–59 y	U-dry	U-dry	0.745	0.996 (dry)	1.000 at P5
Shandong / humidity	20–59 y	Humid-promoting	Humid-promoting	0.922	0.996 (humid)	0.997 at P95
Yunnan / humidity	≥ 60 y	Dry-promoting	Dry-promoting	0.958	0.960 (dry)	0.971 at P5
Hebei / temperature	≥ 60 y	Cold-promoting	Cold-promoting	0.868	0.963 (cold)	0.980 at P5
Hebei / precipitation	≥ 60 y	Heat-promoting	Heat-promoting	0.570	0.872 (wet)	0.971 at P95

Parametric bootstrap: 2,000 draws per province and stratum from the stage-1 reduced coefficient distribution $N(\beta, \hat{V})$; each draw was reconstructed to a full curve and re-classified (see Methods). P(retained): probability of the raw stage-1 shape class; P(direction): probability of the indicated tail direction; P(RR > 1): probability that the relative risk exceeds 1 at the given within-province percentile.

Precipitation

Apodemus-type provinces showed a clear inverted-U precipitation association: risk rose with monthly rainfall to a peak at 175.9 mm (RR 2.73, 95% CI 1.44–5.18) and declined beyond approximately 200 mm (RR at the 95th percentile, 224.5 mm, 2.23, 95% CI 0.66–7.51) (Fig. 1b; Table 2). The association was concentrated in the working-age stratum (peak 190.6 mm, RR 3.08, 95% CI 1.14–8.37), was weaker and unstable at ages ≥ 60 (2.68, 95% CI 0.12–62.61), and was essentially null at ages 0–19 (Fig. 1b). The all-ten-province pooled curve peaked at 168.6 mm (RR 1.78, 95% CI 0.99–3.20) (Table 2). LOPO analysis confirmed that the inverted U did not depend on any single province (RR at the 95th percentile ranging 1.44–3.52). One province-specific feature was robust: in Henan the downturn beyond 200 mm was steeper than elsewhere, and at ages 0–19 the bootstrap dry-direction probability was 0.919 with shape-retention probability 0.821, remaining in the cold(dry)-promoting class under BLUP shrinkage — indicating that the Henan dry-tail collapse is a data-driven feature rather than estimation noise (Table 4; Additional file 1: Table S6). In Hebei (Rattus-type), the precipitation association strengthened with age, from essentially null at ages 0–19 to wet-promoting at ages ≥ 60 (wet-direction probability 0.872; probability that RR exceeded 1 at the 95th percentile 0.971) (Table 4; Additional file 1: Table S6).

Relative humidity

Pooled humidity associations were weak (all-ten-province RR at the 95th percentile, 82.6%, 1.24, 95% CI 0.71–2.15), but province-level directions diverged systematically across climate zones (Fig. 2). In Shaanxi,

all three age strata were dry-promoting with high direction probabilities (0.933, 0.996 and 0.962; at ages 20–59 the probability that RR exceeded 1 at the 5th percentile was 1.000), and Heilongjiang was likewise dry-promoting at ages 0–19 (0.857); in contrast, Shandong was humid-promoting at ages 20–59 and ≥ 60 (0.996 and 0.984), and Liaoning leaned humid at ages 0–19 (0.861) (Table 4; Additional file 1: Table S7). Opposite directions cancelled in the pooled estimate, leaving a near-flat average curve and the largest heterogeneity observed in this study (Apodemus-type all-ages I^2 = 72.8%). Among the Rattus-type provinces, the Yunnan humidity curve was dry-promoting at ages ≥ 60 (direction probability 0.960), whereas Hebei showed a U-dry shape at ages ≥ 60 (dry-direction probability 0.689; probability that RR exceeded 1 at the 5th percentile 0.822).

Age stratification and heterogeneity

Age stratification explained a substantial share of between-province heterogeneity. For Apodemus-type precipitation, I^2 fell from 49.4% in the all-ages analysis to 0% in both the 0–19 and ≥ 60 strata (remaining 54.7% at ages 20–59); temperature showed a similar pattern (Additional file 1: Table S3). Differences in provincial age structure are therefore an important source of the heterogeneity observed in unstratified analyses. Detectable-effect bounds qualified the remaining nulls: at ages 20–59 the pooled MDRs for precipitation were 4.5 (5th percentile) and 9.7 (95th percentile), so effects of the magnitude observed at the curve peak (RR 3.1) were comfortably within reach of the design, whereas MDRs for temperature extremes in sparse strata (for example Mixed-type ages 0–19) exceeded 10^2 (Additional file 1: Table S9), rendering those tail estimates uninformative. Between-stratum MDEs are reported in Additional file 1 (Table S10); tail results should consequently be interpreted within interior percentile ranges.

Drivers of heterogeneity

In univariate meta-regressions (Table 3; Additional file 1: Table S8), heterogeneity of the temperature curves was explained by climatic and demographic background: mean annual temperature (all ages P = 0.0019; ages 20–59 P = 0.00059), centroid latitude (P = 0.0019 and P = 0.00067, respectively), the annualised ageing rate (all ages P = 0.0041, I^2 reduced from 60.0% to 40.2%; ages 20–59 P = 0.0030, residual I^2 20.8%), the 2020 ≥ 60-year population share (P = 0.021 and P = 0.012, respectively) and, at ages 20–59, the urbanisation rate (P = 0.022). Precipitation-curve heterogeneity was associated with the spring-peak share (all ages P = 0.0090; ages 20–59 P = 0.0012), consistent with differing transmission timing under different reservoir seasonality. Humidity-curve heterogeneity was associated with mean annual temperature (all ages P = 0.033; ages 20–59 P = 0.029), corroborating the climate-zone divergence described above.

Table 3
Significant univariate meta-regressions of curve heterogeneity (joint Wald tests)

Exposure	Stratum	Covariate	Wald χ^2	P value	Residual I^2 (%)
Temperature	All ages	Centroid latitude	14.86	0.0019	45.0
Temperature	All ages	Mean annual temperature	14.96	0.0019	45.2
Temperature	All ages	≥ 60 y share 2020	9.72	0.021	50.1
Temperature	All ages	Ageing rate	13.29	0.0041	40.2
Temperature	20–59 y	Centroid latitude	17.13	0.00067	24.9
Temperature	20–59 y	Mean annual temperature	17.39	0.00059	27.5
Temperature	20–59 y	Urbanisation rate 2020	9.67	0.022	31.5
Temperature	20–59 y	≥ 60 y share 2020	10.92	0.012	35.2
Temperature	20–59 y	Ageing rate	13.91	0.0030	20.8
Precipitation	All ages	Spring-peak share	11.57	0.0090	26.1
Precipitation	20–59 y	Spring-peak share	15.92	0.0012	29.9
Relative humidity	All ages	Mean annual temperature	8.77	0.033	46.7
Relative humidity	20–59 y	Mean annual temperature	9.03	0.029	44.1

Univariate multivariate meta-regressions on at most ten provinces; joint Wald tests assess whether the whole exposure–response curve varies with the covariate. Covariates are strongly collinear (latitude versus mean annual temperature); analyses are exploratory.

Robustness

(i) LOPO: Apodemus-type precipitation RRs at the 95th percentile ranged 1.44–3.52 when each province was excluded in turn (Additional file 1: Table S5), so the inverted-U conclusion is not driven by any single province; Mixed-type humidity LOPO was unstable, consistent with the direction mixing described above. (ii) Denominator offset: refitting the all-ages models without the population offset changed point estimates negligibly (Apodemus-type precipitation peak RR 2.73 both with and without the offset), indicating that the qualitative conclusions are insensitive to denominator specification; the value of the offset lies in the rate scale and in enabling age stratification. (iii) Quality control: quality flags removed only four daily records and approximately ten station-months, and one province-month was interpolated, so exposure construction is robust to the quality-control protocol (preliminary versus final exposure series, r = 1.000). (iv) Overdispersion: stratum-level dispersion parameters (0.4–5.6) were accommodated by the quasi-Poisson family. (v) Lag structure: with the cross-basis specification held fixed, the lag pattern (Apodemus-type precipitation peaking at lags of 3–4 months) was unchanged from preliminary analyses.

Discussion

Principal findings

In this two-stage analysis of 132,313 age-stratified HFRS cases across ten Chinese provinces spanning 21 degrees of latitude, meteorological associations were organised along two largely neglected axes. Along the biological axis, pooling by reservoir-host endemic type yielded a coherent and robust inverted-U precipitation association in Apodemus-type provinces, peaking near 176 mm of monthly rainfall and concentrated in the working-age population; by contrast, the two Rattus-type provinces showed opposite temperature-curve directions, demonstrating that host-based typing does not guarantee climatically homogeneous response shapes. Along the demographic axis, age stratification absorbed much of the between-province heterogeneity, and the provincial pace of population ageing remained a leading demographic correlate of the temperature curves alongside climatic background. Humidity showed no consistent average association but a systematic divergence of direction across climate zones — dry-promoting in the semi-arid northwest, humid-promoting in coastal provinces — demonstrating that a single national humidity summary is uninformative.

Comparison with previous evidence

Our results corroborate and extend the recent nationwide case-crossover study by Chang et al. [13] — which analysed 202,154 cases from 285 cities and reported temperature and humidity associations differing across epidemic regions — in four ways. First, whereas that study stratified cities by endemic type, we pooled province-level curves within endemic types on an absolute monthly scale, obtaining an interpretable average curve for the ecologically homogeneous Apodemus-type region. Second, by modelling rates with census-anchored, age-specific denominators and an offset, we ruled out confounding by demographic change and converted their age-subgroup signal into formal age-specific incidence-rate curves; the negligible impact of the offset on point estimates further indicates that, in these data, count-based estimation was not distorted by the absence of denominators. Third, our monthly models with lags of up to six months include precipitation as a main exposure — absent from their main models — and yield threshold-relevant estimates (for example, peak risk near 176 mm monthly precipitation and near 8.7°C) on an absolute scale, complementing their daily, 0–60-day window centred on the incubation period. Fourth, we quantify curve-shape robustness and detectability bounds, providing a framework for interpreting the heterogeneous province-level signals that underlie pooled national estimates. The working-age concentration of the precipitation association is consistent with occupational field exposure during crop cultivation and harvest in Apodemus-endemic farmland [2, 23].

Numerical differences from the nationwide study [13] — for example, its Apodemus-type temperature optimum of 13.7°C versus our 8.7°C — are expected and structural rather than contradictory. Their estimates derive from daily data modelled against fixed reference points (23°C and 75% relative humidity) in a case-crossover design whose same-month controls remove seasonal variation by construction, whereas ours use monthly exposures centred at pooled medians, cumulative lags of 0–6 months and population denominators; curve locations therefore need not coincide.

Mechanisms: precipitation, temperature and reservoir ecology

The inverted-U precipitation curve is biologically plausible for field-rodent-borne transmission. Moderate rainfall supports vegetation, rodent food supply and burrow humidity, raising reservoir density and virus maintenance, whereas excessive rainfall floods burrows, disrupts rodent populations and reduces human field activity, consistent with the downturn beyond approximately 190 mm [5, 6, 9, 20, 21]. The temperature curve peaking near 8.7°C accords with cooler conditions favouring environmental survival of hantaviruses and autumn–winter rodent–human contact around harvest [1, 22, 24–26]. That the ageing rate remained among the strongest demographic correlates of temperature-curve heterogeneity suggests that the temperature sensitivity of HFRS incidence partly reflects the demographic structure of the human population — older rural populations may have higher exposure (continued agricultural work) and higher susceptibility — although this ecological covariate analysis cannot separate these pathways and rests on ten provinces with collinear covariates. The opposite temperature directions of the two Rattus-type provinces — heat-promoting in subtropical Yunnan and cold-promoting in temperate Hebei — are consistent with reservoir and human-activity regimes that differ with climate even under the same dominant host, and caution against pooling spring-peak regions without examining their shapes.

Humidity: divergence across climate zones

The humidity results reconcile apparently conflicting reports in the literature [5, 10] — including the inverted-U humidity association reported for Apodemus-dominant regions at the daily scale [13]: direction itself depends on the climatic context, and region-level averages can conceal divergent provincial directions. In Shaanxi — the driest end of the study transect — dry conditions promoted risk (bootstrap direction probabilities 0.93–1.00), plausibly because low humidity concentrates rodent activity around scarce water and food resources and coincides with the dry autumn–winter transmission season; in coastal Shandong and Liaoning, humid conditions promoted risk, consistent with moisture favouring virus survival and rodent reproduction where baseline humidity is high. Because opposite directions cancel, pooled national estimates of humidity effects are expected to be near-null, exactly as observed here (I^2 = 72.8%). Analyses of humidity–HFRS associations should therefore be climate-zone-stratified by design.

Robustness of province-level shapes

Three province-specific signals survived formal shape-robustness assessment. In Yunnan (Rattus-type), the heat-promoting temperature curve at working ages was retained with probability 0.902 and preserved under BLUP shrinkage; as a spring-peak, commensal-rodent system in a subtropical climate, a high-temperature optimum is coherent. In Hebei, the second Rattus-type province, the temperature curve was instead cold-promoting in all three age strata — most robustly at ages ≥ 60 (shape-retention probability 0.868, cold-direction probability 0.963) — so the two provinces bracket opposite temperature regimes within a single endemic type, and no pooled Rattus-type temperature curve is reported. In Henan, the steep dry-tail downturn of the precipitation curve was retained with probability 0.821 at ages 0–19 and preserved under shrinkage, indicating a data-driven regional feature rather than noise, although its wide intervals warrant confirmation with finer spatial resolution. These examples illustrate the value of quantifying shape

robustness explicitly rather than reading direction off point estimates, particularly where BLUP shrinkage crosses the null.

Null results, detectability and interpretation boundaries

Several associations — notably temperature extremes and most humidity percentiles — were statistically null, but the minimum-detectable-effect analysis shows that these nulls are not equally informative. At working ages the design could detect precipitation RRs of approximately 4.5–9.7 at the 5th and 95th percentiles; the significant inverted-U peak (RR 3.1) lies at interior percentiles where precision is greatest, and the non-significant tails are consistent with these detectability bounds. By contrast, temperature-tail MDRs in sparse strata exceeded 10^2, meaning only implausibly large effects could have been detected there. We therefore restrict interpretation of tail behaviour to interior percentile ranges and report detectability bounds alongside every null — a practice we recommend for multi-region DLNM studies, where tail estimates are notoriously unstable.

Strengths and limitations

Strengths include one of the largest HFRS–meteorology datasets analysed to date (ten provinces, 16 years, three age strata, three exposures), census-anchored population denominators enabling rate-scale estimation, pooling organised by reservoir-host endemic type, explicit shape-robustness quantification combining BLUPs with a 2,000-draw parametric bootstrap, and detectability bounds for null results. Several limitations apply. First, the ecological design at province-month resolution entails exposure misclassification and ecological fallacy; province-level aggregation may mask within-province contrasts, particularly in large provinces spanning several climate zones. Second, the Mixed-type group comprised three provinces with divergent shapes, and its pooled curves were unstable; likewise the two Rattus-type provinces showed opposite temperature-curve directions, so Rattus-type results are reported per province and no pooled Rattus-type estimate is given. Third, sparse strata (0–19 years, and all strata in low-incidence provinces) yielded wide intervals, which we addressed through MDRs rather than over-interpretation. Fourth, meta-regressions rested on at most ten provinces with strongly collinear covariates and are hypothesis-generating. Fifth, we did not model reservoir density, land use, vaccination or rodent-control programmes, which may confound or mediate meteorological associations. Finally, HFRS reporting may vary across provinces and over time, although the notifiable-disease system and case definition were stable over the study period.

Conclusions

Across ten Chinese provinces during 2005–2020, meteorological associations with HFRS incidence were structured by reservoir-host endemic type and concentrated in the working-age population. Moderately high monthly precipitation (around 176 mm) was associated with the highest risk in Apodemus-type regions, temperature risk peaked near 8.7°C, and humidity effects diverged in direction across climate zones, precluding a single national summary. The two Rattus-type provinces exhibited opposite temperature-curve shapes, underscoring climatic heterogeneity within an endemic type. Population ageing modified the temperature association, linking a major demographic transition to a climate-sensitive zoonosis. Age-stratified designs with population denominators, endemic-type pooling and explicit shape-robustness and

detectability assessment provide a transferable framework for multi-region studies of climate-sensitive infectious diseases.

Abbreviations

BLUP
best linear unbiased prediction
CI
confidence interval
DLNM
distributed lag non-linear model
HFRS
haemorrhagic fever with renal syndrome
HTNV
Hantaan virus
I^2
I-squared statistic
LOPO
leave-one-province-out
MDE
minimum detectable effect
MDR
minimum detectable relative risk
P5/P25/P50/P75/P95
5th/25th/50th/75th/95th percentiles
QC
quality control
RH
relative humidity
RR
relative risk
SEOV
Seoul virus.

Declarations

Ethics approval and consent to participate

Not applicable. The study used aggregated, anonymised surveillance counts and publicly available census and meteorological data; no individually identifiable information was accessed, and ethical approval and informed consent were not required.

Consent for publication

Not applicable.

Clinical trial number

Clinical trial number: not applicable. This was an ecological analysis of routinely collected, aggregated surveillance data; no trial participants were enrolled, allocated, or followed up.

Competing interests

The authors declare that they have no competing interests.

Funding

This work was financially supported by the Natural Science Basic Research Program Youth Project of Shaanxi Provincial Science and Technology Department (No. 2023-JC-QN-0830). The sponsors had no role in the study design and in the collection, analysis, and interpretation of data.

Author Contribution

FW, MT and ZT conceived and designed the study. FW, MT and YL acquired the surveillance, meteorological and census data and curated the analysis datasets. FW performed the statistical analysis and drafted the manuscript, with methodological support from MT and YL. MK and YL contributed to data validation, quality control and the literature review. YD contributed virological and surveillance expertise and assisted with acquisition and interpretation of the surveillance data. MT verified the underlying data and contributed to drafting and revision of the manuscript. TC and ZT supervised the study, contributed to the interpretation of the results and critically revised the manuscript for important intellectual content. ZT acquired the funding and is the guarantor of the work. FW and MT contributed equally to this work and share first authorship. All authors read and approved the final manuscript.

Acknowledgement

We thank the Data-center of China Public Health Science and the National Tibetan Plateau / Third Pole Environment Data Center for data access.

Availability of data and materials

HFRS case data were obtained from the Data-center of China Public Health Science (https://www.phsciencedata.cn) and are available from that source subject to its data-use agreement; The meteorological data were obtained from the China Meteorological Administration SURF_CLI_CHN_MUL_DAY V3.0 dataset via the National Tibetan Plateau / Third Pole Environment Data Center (http://data.tpdc.ac.cn);

Census tabulations are published by the National Bureau of Statistics of China. The analytic dataset and R code are available from the corresponding author on reasonable request.

References

1. Jonsson CB, Figueiredo LTM, Vapalahti O. A global perspective on hantavirus ecology, epidemiology, and disease. Clin Microbiol Rev. 2010;23(2):412–41.
2. Zhang S, Wang S, Yin W, Liang M, Li J, Zhang Q, et al. Epidemic characteristics of hemorrhagic fever with renal syndrome in China, 2006–2012. BMC Infect Dis. 2014;14:384.
3. Wen B, Yang Z, Ren S, Fu T, Li R, Lu M, et al. Spatial-temporal patterns and influencing factors for hemorrhagic fever with renal syndrome: a 16-year national surveillance analysis in China. One Health. 2024;18:100725.
4. Hansen A, Cameron S, Liu Q, Sun Y, Weinstein P, Williams C, et al. Transmission of haemorrhagic fever with renal syndrome in China and the role of climate factors: a review. Int J Infect Dis. 2015;33:212–8.
5. Xiao H, Tian HY, Cazelles B, Li XJ, Tong SL, Gao LD, et al. Atmospheric moisture variability and transmission of hemorrhagic fever with renal syndrome in Changsha City, Mainland China, 1991–2010. PLoS Negl Trop Dis. 2013;7(6):e2260.
6. Zhang WY, Gu WD, Fang LQ, Li CP, Bi P, Glass GE, et al. Climate variability and hemorrhagic fever with renal syndrome transmission in Northeastern China. Environ Health Perspect. 2010;118(7):915–20.
7. Fang LQ, Wang XJ, Liang S, Li YL, Song SX, Zhang WY, et al. Spatiotemporal trends and climatic factors of hemorrhagic fever with renal syndrome epidemic in Shandong Province, China. PLoS Negl Trop Dis. 2010;4(8):e789.
8. Wei Y, Wang Y, Li X, Qin P, Lu Y, Xu J, et al. Meteorological factors and risk of hemorrhagic fever with renal syndrome in Guangzhou, southern China, 2006–2015. PLoS Negl Trop Dis. 2018;12(6):e0006604.
9. Bi P, Wu X, Zhang F, Parton KA, Tong S. Seasonal rainfall variability, the incidence of hemorrhagic fever with renal syndrome, and prediction of the disease in low-lying areas of China. Am J Epidemiol. 1998;148(3):276–81.
10. Cao L, Huo X, Xiang J, Lu L, Liu X, Song X, et al. Interactions and marginal effects of meteorological factors on haemorrhagic fever with renal syndrome in different climate zones: evidence from 254 cities of China. Sci Total Environ. 2020;721:137564.
11. Luo Y, Zhang L, Xu Y, Kuai Q, Li W, Wu Y, et al. Epidemic characteristics and meteorological risk factors of hemorrhagic fever with renal syndrome in 151 cities in China from 2015 to 2021: retrospective analysis. JMIR Public Health Surveill. 2024;10:e52221.
12. Wang Y, Zhang C, Gao J, Chen Z, Liu Z, Huang J, et al. Spatiotemporal trends of hemorrhagic fever with renal syndrome (HFRS) in China under climate variation. Proc Natl Acad Sci U S A. 2024;121(4):e2312556121.
13. Chang N, Huang W, Niu Y, Xu Z, Gao Y, Ye T, et al. Risk of hemorrhagic fever with renal syndrome associated with meteorological factors in diverse epidemic regions: a nationwide longitudinal study in China. Infect Dis Poverty. 2025;14(1):3.

14. Data-center of China Public Health Science. Hemorrhagic fever with renal syndrome surveillance data. Beijing: National Population Health Data Center. https://www.phsciencedata.cn. Accessed [date].
15. National Bureau of Statistics of China. Tabulations of the 2000, 2010 and 2020 Population Censuses of China. Beijing: China Statistics.
16. China Meteorological Data Sharing Service System. Daily surface climate dataset of China (SURF_CLI_CHN_MUL_DAY), version 3.0. https://data.cma.cn/en. Accessed [date].
17. Gasparrini A, Armstrong B, Kenward MG. Distributed lag non-linear models. Stat Med. 2010;29(21):2224–34.
18. Gasparrini A. Modeling exposure-lag-response associations with distributed lag non-linear models. Stat Med. 2014;33(5):881–99.
19. Gasparrini A, Armstrong B, Kenward MG. Multivariate meta-analysis for non-linear and other multi-parameter associations. Stat Med. 2012;31(29):3821–39.
20. Wang L, Wang T, Cui F, Zhai SY, Zhang L, Yang SX, et al. Hemorrhagic fever with renal syndrome, Zibo City, China, 2006–2014. Emerg Infect Dis. 2016;22(2):274–6.
21. Xue C, Zhang B, Li Y, Li X, Xu C, Wang Y. Asymmetric association between meteorological factors and human infections with hemorrhagic fever with renal syndrome: a 16-year ecological trend study in Shaanxi, China. One Health. 2024;19:100895.
22. Wang Y, Zhang B, Xue C, Zhou P, Dong X, Xu C, et al. Long- and short-run asymmetric effects of meteorological parameters on hemorrhagic fever with renal syndrome in Heilongjiang: a population-based retrospective study. Transbound Emerg Dis. 2024;2024:6080321.
23. Bi P, Tong S, Donald K, Parton K, Ni J. Climatic, reservoir and occupational variables and the transmission of haemorrhagic fever with renal syndrome in China. Int J Epidemiol. 2002;31(1):189–93.
24. Wei X, Xiao X, Yin W, He J, Ren Z, Li Z, et al. Climate and socio-economic factors drive the spatio-temporal dynamics of HFRS in Northeastern China. One Health. 2022;15:100466.
25. Vaheri A, Strandin T, Hepojoki J, Sironen T, Henttonen H, Mäkelä S, et al. Uncovering the mysteries of hantavirus infections. Nat Rev Microbiol. 2013;11(8):539–50.
26. Tian H, Stenseth NC. The ecological dynamics of hantavirus diseases: from environmental variability to disease prevention largely based on data from China. PLoS Negl Trop Dis. 2019;13(2):e0006901.
27. Sera F, Armstrong B, Blangiardo M, Gasparrini A. An extended mixed-effects framework for meta-analysis. Stat Med. 2019;38(29):5429–44.
Note. all journal references were verified against publisher or PubMed records (28 September 2026); access dates for references 14 and 16 to be inserted at submission.

Figures

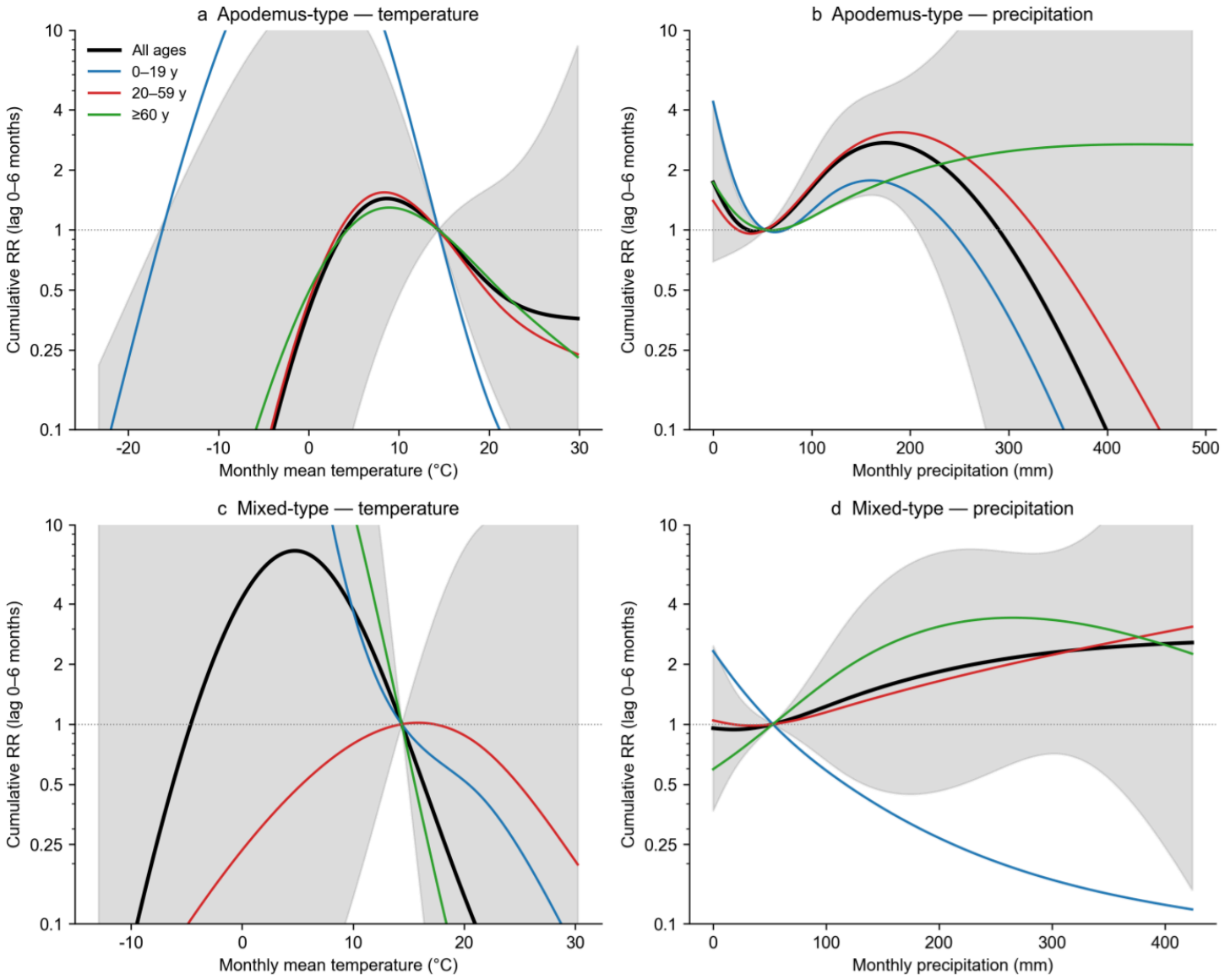


Figure 1

Pooled cumulative exposure–response curves for temperature and precipitation by endemic type

Cumulative relative risks (RRs, lag 0–6 months) of HFRS incidence associated with monthly mean temperature (a, c) and monthly total precipitation (b, d), pooled across Apodemus-type provinces (Heilongjiang, Shaanxi, Shandong, Jiangxi, Henan; a, b) and Mixed-type provinces (Liaoning, Hunan, Sichuan; c, d). Black lines: all ages; blue: 0–19 years; red: 20–59 years; green: ≥60 years. Shaded areas are 95% confidence intervals for the all-ages estimate. Curves are centred at the pooled median exposure; the y-axis is on the log scale. Estimates derive from two-stage distributed lag non-linear models with random-effects multivariate meta-analysis, 2005–2020.

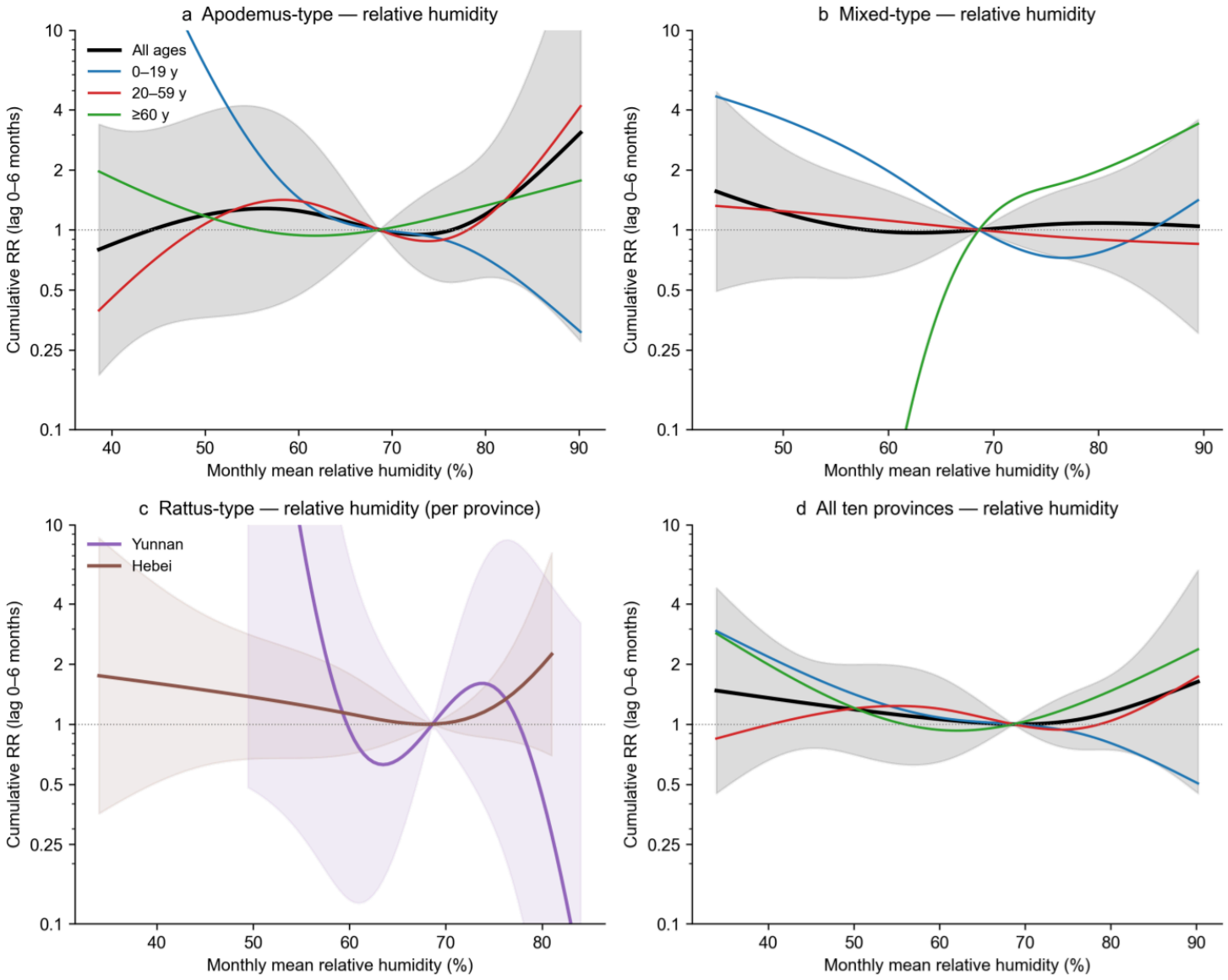


Figure 2

Pooled cumulative exposure–response curves for relative humidity by analytic group

Cumulative RRs (lag 0–6 months) for monthly mean relative humidity in Apodemus-type provinces (a), Mixed-type provinces (b), the two Rattus-type provinces (c; per-province stage-1 all-ages estimates without random-effects pooling, because the provincial curves diverged; purple: Yunnan; brown: Hebei) and all ten provinces (d). Line colours and shading in panels a, b and d as in Fig. 1. Models adjusted for monthly mean temperature and total precipitation. Direction divergence across climate zones (dry-promoting versus humid-promoting) produces the near-flat pooled curves.

Supplementary Files

This is a list of supplementary files associated with this preprint. Click to download.

- HFRS10provIDPAdditionalfile1.docx